

SCM – A SOIL CONTACT MODEL FOR MULTI-BODY SYSTEM SIMULATIONS

Rainer Krenn¹ and Gerd Hirzinger¹

¹ German Aerospace Center (DLR), Institute of Robotics and Mechatronics, Oberpfaffenhofen, 82234 Wessling, Germany
rainer.krenn@dlr.de, gerd.hirzinger@dlr.de

Abstract

The paper introduces a new simulation tool called *Soil Contact Model (SCM)* that has been recently developed at DLR's *Institute of Robotics and Mechatronics*. SCM provides an interface between the classical terramechanics theory of Bekker and the capabilities of multi-body system (MBS) simulation technique for general, full 3D simulations of soil contact dynamics problems. Beyond the computation of contact forces and torques, a further key component of SCM is the computation of plastic soil deformation during physical contact with wheels, tracks, legs or any other arbitrarily shaped contact objects. It comprises features such as generation of the contact footprint, displacement of soil material and landfill around the contact zone. These features enable SCM to compute typical terramechanical phenomena like (1) rising rolling resistance caused by humps in front, (2) lateral guidance inside ruts, (3) drawbar pull variations versus slippage and (4) multi-pass effects of wheels running inline. Unlike volumetric, FEM/DEM-like approaches SCM computes all required data based on relative kinematics between discretized contact surfaces. Therefore, the computational efficiency is quite high and adequate for MBS applications. In the paper the architecture and the key features of the implementation are presented. Simulation performance and sensitivity aspects of SCM are addressed in chapters on verification and correlation with experimental results.

Keywords: Multi-Body System Simulation, Contact Dynamics, Soil Contact Model

1 Introduction and Motivation

In the recent years robot mobility has become an increasingly important issue in space robotics. Locomotion and navigation on rough, unstructured terrain is one of the major challenges in this field of research.

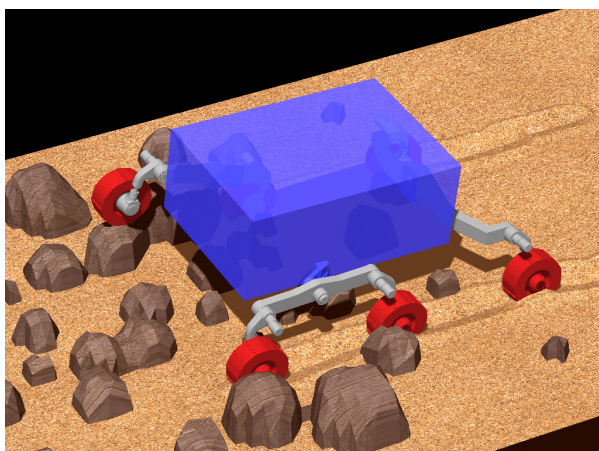


Fig. 1: Locomotion simulation of ExoMars rover

The *Institute of Robotics and Mechatronics* at DLR is involved in robotics mobility development through a

number of activities like vision based navigation and mobile platform design. Moreover, the simulation of mobile systems plays an important role as well. For the specific problem of mobility on sandy, planetary terrain a new simulation tool called *Soil Contact Model (SCM)* was recently developed and already applied for the prediction and verification of the ExoMars (ESA) rover locomotion performance (Fig. 1).

2 Overview of SCM

As a first and very general definition we can formulate: SCM makes the classical terramechanics theory, developed by Bekker [1] and referenced in publications of Wong [2], compatible for the specific capabilities of the multi-body system (MBS) simulation technique, which can be characterized as a very good compromise between system complexity reduction, simulation accuracy and computational performance. In Fig. 2 a simplified MBS model of a rover is pictured, whereas only one wheel system is explicitly shown. It is assembled by MBS library objects. The major ones are body objects (blue) and joint objects (green), which together define the kinematics tree of the system, and force objects (red), which are used to apply forces and torques to the bodies depending on their specific implementation (e.g. friction, actuators, contact forces).

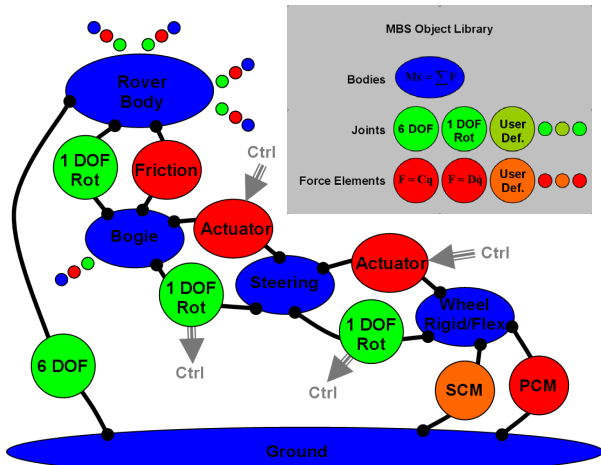


Fig. 2: Location of SCM within MBS Model

From the MBS library point of view SCM is a specific force object for computing full 3D contact forces and torques between an arbitrarily shaped contact object and a terrain of plastically deformable soil. From the coding point of view SCM can be described as a function (subroutine) with the following interface:

- Input Arguments: Relative pose and relative linear and angular velocities between contact object and soil.
- Output Arguments: Contact forces and torques between contact object and soil.

- Parameters: Surface shapes of contact object and soil, soil parameters.

Accordingly, SCM is typically called by the MBS solver at each time integration step of the MBS simulation run. But it can be used offline, respectively outside the MBS context as well. The overall architecture of the SCM function is presented in Fig. 3.

3 Details of SCM Implementation

Inside the SCM function two tasks are performed at each function call, respectively at each MBS solver step (see Fig. 3):

1. The computation of contact forces and torques between contact object and soil as function of the contact parameters and the relative kinematics between the contact object and the soil (green block of Fig. 3).
2. The computation of the plastic soil deformation during contact (yellow block of Fig. 3). This feature plays an essential role for the correct representation of terramechanical phenomena like bulldozing or multi-pass effects and their dynamics impact during simulation.

The details of the SCM implementation will be introduced in the following chapters.

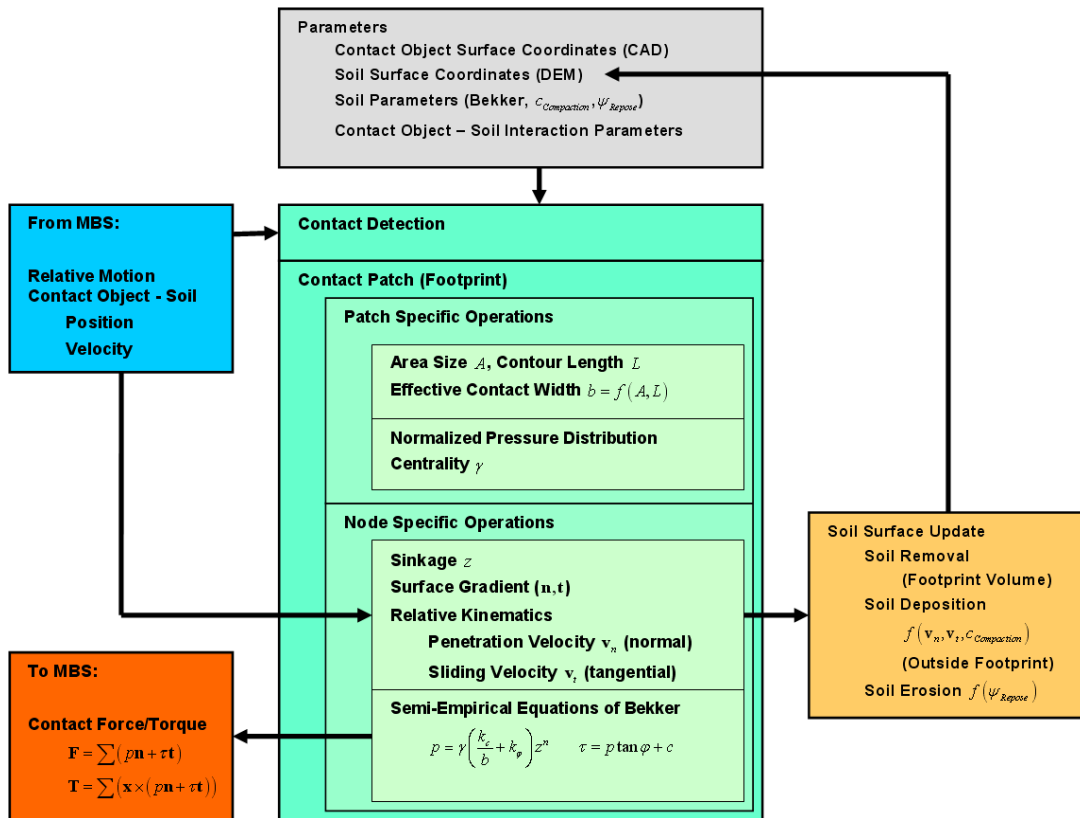


Fig. 3: Architecture of SCM

3.1 SCM Function Parameters

The parameters of the SCM-function are the followings:

1. Soil surface description,
2. Soil dynamics parameters,
3. Contact object surface description,
4. Surface friction parameters.

Soil surface description:

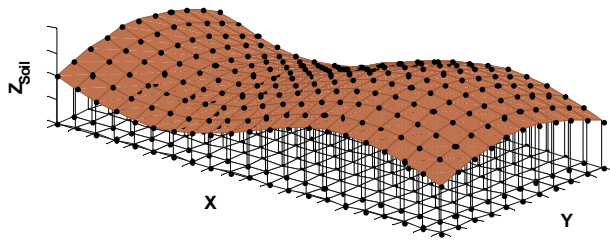


Fig. 4: DEM of soil surface

For use within SCM the soil surface has to be described as a Digital Elevation Model (DEM) with a regularly spaced ($dx = dy = ds$) horizontal mesh grid (Fig. 4) and with the elevation coordinate axis in parallel to the gravity vector. Each grid node is representing a discrete part $dA = ds^2$ of the soil area and the corresponding surface height. The granularity of the grid should be small enough in order to represent the soil topology with a sufficient accuracy, even after plastic deformation.

Soil dynamics parameters:

Each grid node of the soil is associated with five soil dynamics parameters, which are required to apply Bekker's terramechanics theory during the contact dynamics computations. They can be globally defined for the entire soil area or individually for each grid node. These classical Bekker parameters are specified in Table 1. Furthermore, the soil's maximum angle of repose ψ has to be introduced.

Table 1: Soil Parameters

Exponent of sinkage	n	[-]
Cohesive modulus	k_c	[N/m ⁿ⁺¹]
Frictional modulus	k_ϕ	[N/m ⁿ⁺²]
Cohesion	c	Pa
Angle of internal friction	ϕ	[-]

The bulk density of the soil or similar inertia specific data must not be defined explicitly since they are already implicitly included in the soil parameters of Table 1.

Contact object surface description:

The contact body has to be described as an ordinary polygonal mesh (Fig. 5) that defines its outer surface

by faces and vertices, while the maximum face edge length should not exceed the mesh grid width of the soil for successful contact detection. The body inertia that is part of the MBS body object parameters is not taken into account in the SCM parameters.

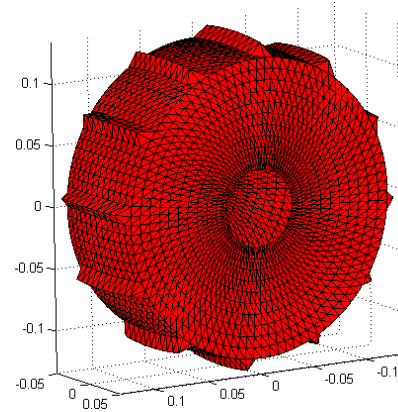


Fig. 5: Polygonal surface representation of the contact object

Friction Parameters:

The Coulomb friction between the surfaces of soil and contact object is considered by a friction coefficient μ .

3.2 SCM Force/Torque Computation

The first SCM-function task is the computations of contact forces and torques between the contact object and the soil. The algorithm can be divided in three major parts (see Fig. 3):

1. Contact detection between contact object and soil and footprint definition,
2. Footprint specific computations.
3. Footprint node specific computations,

We can describe this part of the code generally as a preparation of the available contact information in order to apply finally Bekker's well known pressure-sinkage relationship

$$p = \left(\frac{k_c}{b} + k_\phi \right) z^n \quad (1)$$

with

p : mean probe contact pressure,

b : width/radius of footprint,

z : sinkage of footprint.

and with the soil parameters k_c , k_ϕ and n according to Table 1. However, this formula is only valid for a small range of applications, e.g. bevameter tests with circular probes and flat probe faces. Therefore, the basic task of this SCM part is the adaptation and extension of (1) for arbitrarily shaped footprints and contact kinematics.

Contact Detection:

The contact detection starts with a transformation of the contact object vertices according to the contact object pose computed by the MBS solver. In the next step the transformed vertices are mapped into the soil grid space such that they are arranged in columns at soil grid node locations. The minimum of each column is a potential candidate for contact with the soil and the actual contact can be detected simply by comparing the vertical coordinate of the column minimum with the height at the corresponding soil grid node. The output of this procedure is a discretized footprint (intersection volume) of the contact object in the soil. The sequence of the contact detection is presented in Fig. 6.

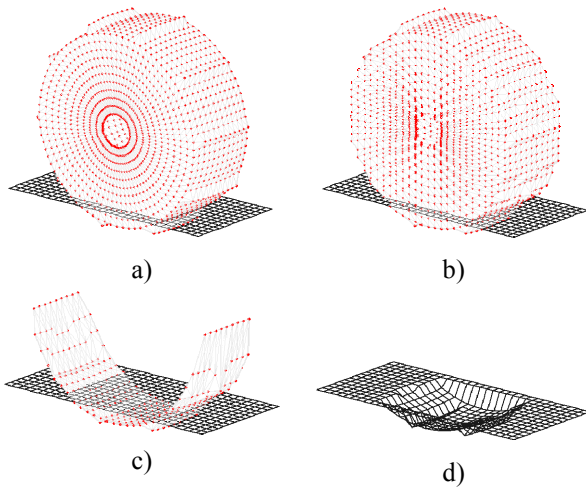


Fig. 6: Contact detection procedure in SCM

Footprint Node Specific Computations:

After contact detection, respectively footprint definition, SCM can directly compute a set of individual footprint node information to be used in the subsequent computations of contact stress and force/torque:

z_i : sinkage,

\mathbf{v}_i : contact velocity,

\mathbf{n}_i : contact surface normal vector,

\mathbf{t}_i : contact surface tangential vector.

Footprint Specific Computations:

In the first footprint specific computation SCM derives the effective contact width b_{eff} to be applied in (1) for the general contact case. Taking into account, that (1) was developed based on bevameter experiments using circular probes with

$b = r$: probe face radius,

$A = r^2\pi$: probe face area size,

$L = 2r\pi$: probe face contour length,

Eq. (1) can be expressed in the force domain as well by

$$F = Ap = \left(L \frac{k_c}{2} + Ak_\phi \right) z^n. \quad (2)$$

However, in contrast to b , A and L can be numerically computed and tracked independent from the actual footprint shape. This fact is exploited in SCM and following, the contact width is expressed by

$$b_{eff} = \frac{2A}{L}. \quad (3)$$

Eq. (3) is formally exact for circular and slim rectangular probes and is a good approximation for general cases of convex footprints. The discrete approximations of A and L are computed by

$$A = \left(\sum_{i=1}^{n_{Contact}} c_{A,Contact,i} + \sum_{j=1}^{n_{Contour}} c_{A,Contour,j} \right) dA \quad (4)$$

and

$$L = \left(\sum_{i=1}^{n_{Contact}} c_{L,Contact,i} + \sum_{j=1}^{n_{Contour}} c_{L,Contour,j} \right) ds. \quad (5)$$

The weighting factors c_A and c_L are considering the individual location type of the grid nodes inside the footprint and along the footprint contour. In Fig. 7 the types of contact nodes (inside discrete footprint, red) and contour nodes (footprint border, blue) are explained for an arbitrary footprint shape. In SCM, the node type classification depends on the number of contact nodes in the direct neighbourhood.

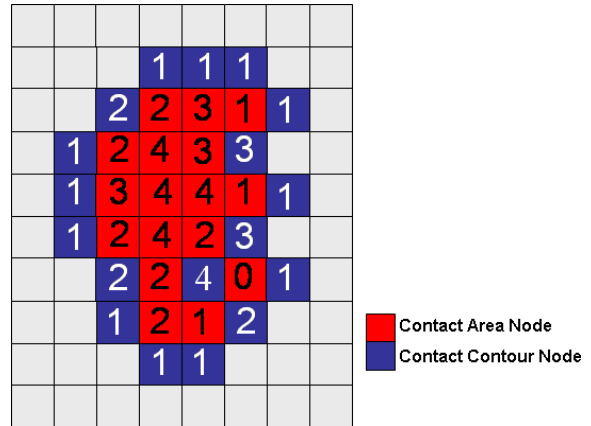


Fig. 7: Node classification of discrete contact footprint

A second part of footprint specific computations takes into account that the pressure distribution in a footprint is generally not constant, even in case of flat footprints. This fact is relevant for correct computation of contact torques (e.g. steering resistance) and sinkage of convex contact objects.

Basically, the pressure drops from central regions to the border of the footprint, which is considered in SCM by a weighting factor to be multiplied by the contact pressure as introduced in (1). The individual weighting factor γ_i at a grid node depends on its centrality inside the footprint and the balance of internal soil friction and cohesion. It is introduced in simplified form in Eq. (6).

$$\gamma_i = \frac{n_{\text{Contact}} w_i}{w_{\text{Total}}}; \quad \left\{ \begin{array}{l} w_i = \sum_{j=1, j \neq i}^{n_{\text{Contact}}} \frac{1}{\text{fcn}(|\mathbf{r}_j - \mathbf{r}_i|, c, \varphi)} \\ w_{\text{Total}} = \sum_{i=1}^{n_{\text{Contact}}} w_i \end{array} \right. \quad (6)$$

The mean value of γ is 1. In Fig. 8 the SCM pressure distribution functions of a circular footprint for two different soil conditions are presented. In case of dominant internal friction (e.g. dry sand) the pressure distribution is flat with a maximum value $\gamma_{\max} \approx 1$. In case of dominant cohesion (e.g. saturated clay) the function rises continuously from border to centre and obtains its maximum at $\gamma_{\max} \approx 2$. These numerical results match quite well with the theory as published in [3].

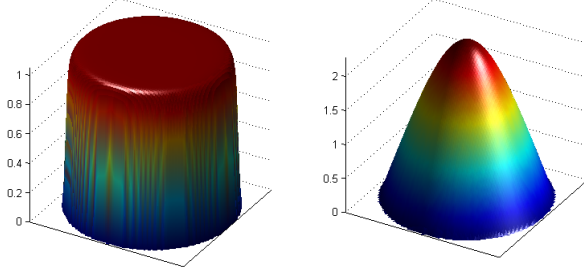


Fig. 8: Pressure distribution of circular footprints
Left: Dominant internal friction φ
Right: Dominant cohesion c

An example for the pressure distribution of a non-circular, discontinuous footprint area is shown in Fig. 9, which should represent the general case (e.g. wheel profile, track profile) as processed in SCM.

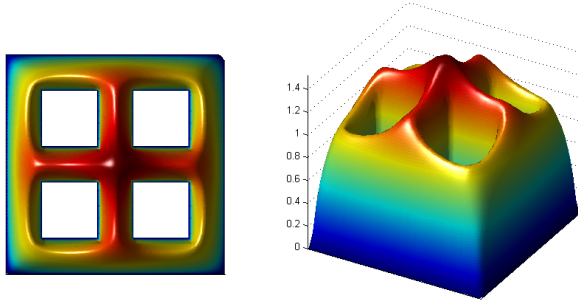


Fig. 9: Pressure distribution of a non-circular footprint

Contact Pressure and Contact Force:

After the introduced preparation steps SCM is computing the local contact pressure at a footprint grid node by

$$p_i = \gamma_i \left(\frac{k_c}{b_{\text{eff}}} + k_\varphi \right) z_i^n \quad (7)$$

Supposed that the lengths of \mathbf{n}_i and \mathbf{t}_i are equal to the corresponding discrete contact surface size, which is represented by the grid node, the description of the local contact force is the following:

$$\mathbf{F}_i = \begin{pmatrix} c \\ c \\ 0 \end{pmatrix} + p_i \begin{pmatrix} \tan \varphi & 0 & 0 \\ 0 & \tan \varphi & 0 \\ 0 & 0 & 1 \end{pmatrix} \mathbf{n}_i + \mu p_i \mathbf{t}_i \quad (8)$$

Herein, two components of shear stress are implemented:

1. The Mohr-Coulomb failure criterion for soil $\tau_1 = c + p \tan \varphi$ and
2. The Coulomb friction between sliding surfaces $\tau_2 = p \mu$.

The total contact forces and torques are computed by discrete integrations over the entire footprint area:

$$\mathbf{F}_{\text{Total}} = \sum_{i=1}^{n_{\text{Contact}}} \mathbf{F}_i; \quad \mathbf{T}_{\text{Total}} = \sum_{i=1}^{n_{\text{Contact}}} (\mathbf{r}_i \times \mathbf{F}_i) \quad (9)$$

3.3 SCM Plastic Soil Deformation

The computation of plastic soil deformation is an essential pre-requisite for correct simulation of typical terramechanical phenomena like

- Bulldozing: Increased rolling resistance caused by humps in front,
- Multi-Pass: Reduced rolling resistance in pre-deformed ruts,
- Lateral guidance inside ruts,
- Drawbar pull as function of slippage.

Soil volume deformation problems as well known from civil engineering are typically solved using *Finite Element Model* or *Discrete Element Model* techniques. However, due to the extreme computational load of these methods they are not applicable for time-efficient MBS simulations.

Soil Displacement:

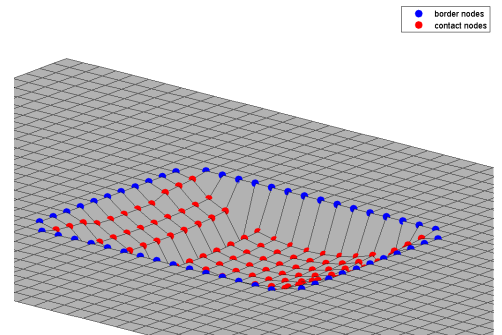


Fig. 10: Soil DEM with integrated footprint

In SCM a computationally very efficient technique for manipulating the DEM of the soil is implemented. It supposes that a node specific amount of soil

$$dV_i = z_i dA, \quad (10)$$

which depends on the local sinkage and the area size of a soil grid raster element, has to be displaced. Thus, the first simple DEM manipulation is the integration of the footprint as shown in Fig. 10.

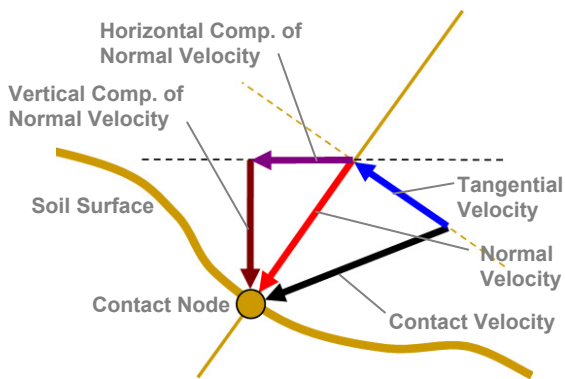


Fig. 11: Contact kinematics at contact node

The applied displacement law depends on the local contact velocity at a contact grid node (see Fig. 11). It is supposed that only normal components of the contact velocity are related to soil penetration and therefore only this component is relevant for soil displacement.

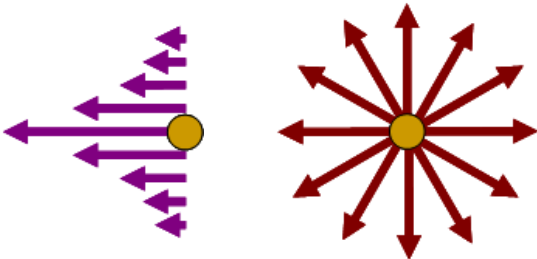


Fig. 12: Soil flow fields
 Left: Parallel field caused by bulldozing
 Right: Radial field caused by sinkage

Considering only the normal velocity we can divide it into two components:

1. Horizontal component of normal velocity:
 It causes bulldozing effects and the corresponding local soil flow field is therefore modelled as a parallel field according to Fig. 12 left.
2. Vertical component of normal velocity:
 It causes the vertical displacement of the soil. Under the assumption of incompressible soils we consequently obtain a local radial soil flow field as pictured in Fig. 12 right.

The ratio of the field strengths is supposed to be equal to the ratio of the corresponding penetration velocity components.

Soil Deposition:

The deposition of the displaced soil, respectively the manipulation of the corresponding DEM regions is implemented in two steps: In a first temporary step the soil is banked up at the border of the footprint as shown in Fig. 13. Hereby, each border node receives a portion of soil from each contact node, depending on the local intensities of the soil flow fields at the footprint border.

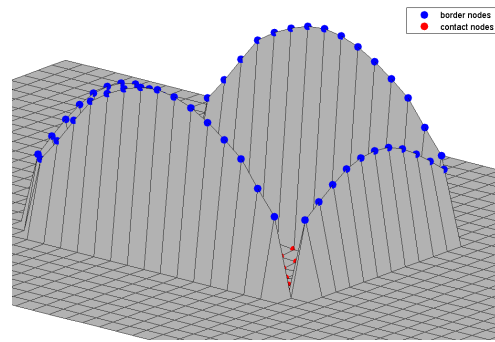


Fig. 13: Temporary soil DEM appearance

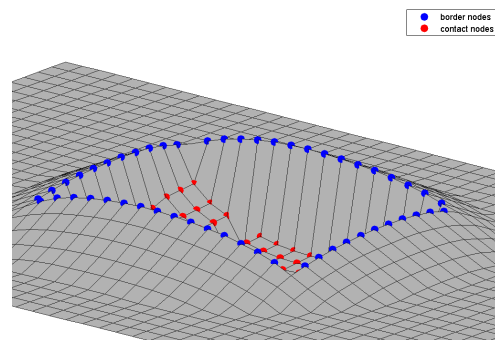


Fig. 14: Final soil DEM shape after erosion

The DEM manipulation is finished after applying an erosion algorithm (second step of soil deposition) that distributes the soil in the vicinity of the footprint under the constraint that the maximum DEM inclination is smaller than the maximum soil specific angle of repose.

The updated DEM is stored by SCM (see Fig. 3) and applied at the next call as initial soil surface description for contact force computations according to chapter 3.2.

4 Verification of SCM

In the model verification process the correctness of the implementation and the fidelity of implemented theory has to be proven. In case of SCM it should be taken into account that Bekker's ideal pressure sinkage relationship according to (1), which is the kernel of the SCM dynamics computations, was originally derived from results of bevameter experiments. Accordingly, for verification purposes it is valid and appropriate to compare the ideal results of (1) with the SCM simulation results of bevameter experiment models. The verification is successful if both, the generation of the pressure sinkage relationship and the identification of the applied soil parameters are possible with sufficient accuracy.

In Fig. 15 the simulation results for different probe sizes and grid resolutions are presented and compared with the ideal force-sinkage relationship of Bekker.

The discrepancies of the results are caused by the inaccuracies at the discrete computation of footprint area size A and contour length L (see Fig. 7), which strongly influence the accuracy of b_{eff} . Therefore, the best results can be obtained if the number of grid

nodes, which define the outer contour of the footprint, is relatively small compared with the number of nodes inside the footprint area (large footprint area at high grid resolution, see Fig. 15, bottom right).

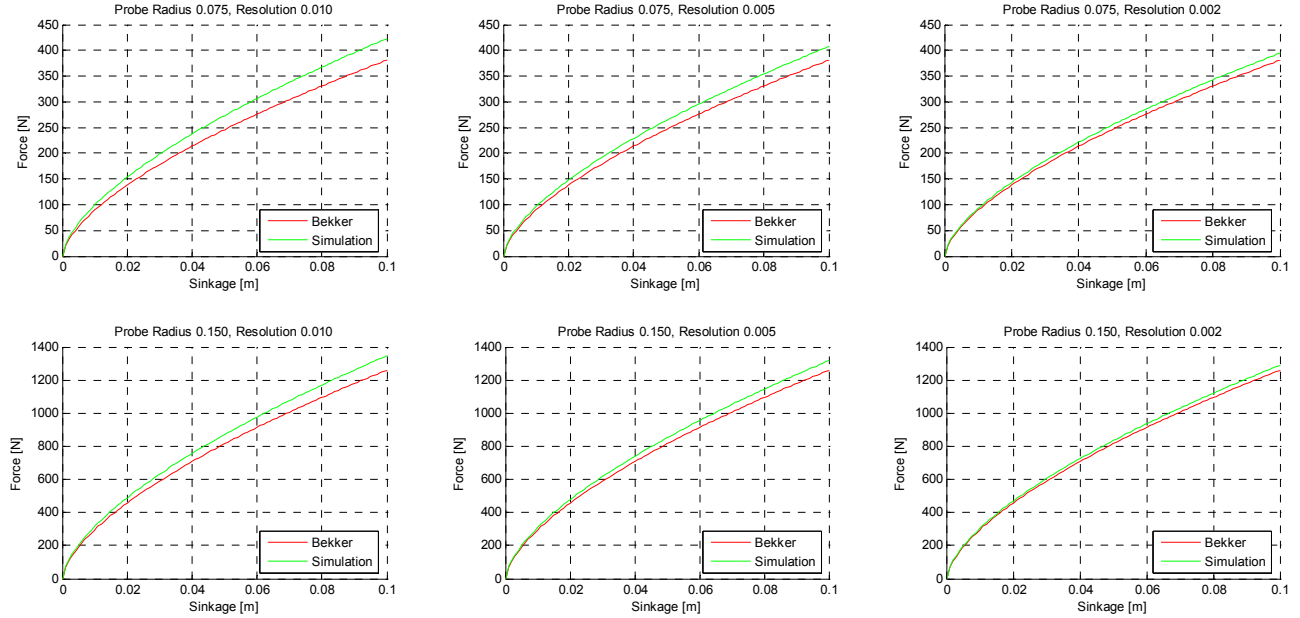


Fig. 15: Ideal and simulated force-sinkage relationship
 Footprint radius: Top/bottom = 0.075/0.15 m. Soil grid resolution: Left/center/right = 0.01/0.005/0.002 m
 Applied soil parameters: Mars soil simulant DLR-A [4]

In the second verification step the soil parameters are identified based on the simulation results shown in Fig. 15 (including the discrete approximations of A , L and b).

Table 2: Identified soil parameters

Parameter	k_c	k_ϕ	n
Applied, Simulant DLR-A	2370	60300	0.63
Identified, $ds = 0.010$	2398	60159	0.63
Identified, $ds = 0.005$	2377	60260	0.63
Identified, $ds = 0.002$	2371	60293	0.63

The results are collected in Table 2. Obviously, they match quite well with the actual applied ones and therefore it is valid to assume that no further critical details are “hidden” in the current SCM implementation.

5 Correlation with System Level Tests

The verification of SCM as described in the previous chapter is a formal prove of model correctness. However, it doesn't say anything about the general applicability to any soil contact simulation task. Therefore, the performance of SCM should be demonstrated and discussed using an application example. For correlation

purposes the results of the ExoMars rover system level tests (conducted by ETH Zurich at Oerlikon Space, Zurich, [5]) have been taken as reference. One of the tests in this campaign was the measurement of the drawbar pull of the rover. This value is typically a function of wheel slippage. In order to generate well defined slippage conditions during the experiment the rover was tethered while cruising in the testbed that was filled up with Mars soil simulant. The slippage s was adjusted by tuning the ratio between the roll-up velocity of the tether and the nominal rover velocity according to the following equation:

$$s = 1 - \frac{v_{Tether}}{v_{Rover,nominal}} = 1 - \frac{v_{Tether}}{\omega_{Wheel} r_{Wheel}} \quad (11)$$

with

v_{Tether} : Roll-off velocity of tether,

ω_{Wheel} : Angular velocity of rover wheels,

r_{Wheel} : Radius of rover wheels.

For each experiment, respectively simulation run, the slippage was kept constant. The measured drawbar-pull forces were recorded as function over time. For presentation purposes these functions were scaled in time, placed inside a single diagram and graphically connected in order to obtain the functions of drawbar-pull versus slippage. In Fig. 16 the corresponding results of the ExoMars test campaign and the SCM simu-

lation runs are presented. The discussion of the simulation results has to take two aspects into account:

1. The SCM simulation results (blue) generate a “classical” (see [6]) function of drawbar pull versus slippage with asymptotical approach to the maximum value and match quite well with the results of the experiments (green) in the range of $s > 40\%$. However, the discrepancies for smaller slippage are significant, which refers to the next aspect.
2. Bekker’s pressure-sinkage relationship (1) does not take velocity dependent terms explicitly into account. On the other hand, SCM has to do it for simulation stability reasons and is therefore apply-

ing a preliminary, soil physics independent, linear damping component for contact force computations. The influence of the damping can be demonstrated by running the same simulations at a higher velocity level (red graph in Fig. 16). Under the new conditions the matching range can be extended significantly and following it is reasonable to suppose that a good match over the entire slippage range could be achieved if the well known set of Bekker soil parameters (Table 1) will be extended by appropriate, velocity dependent parameters.

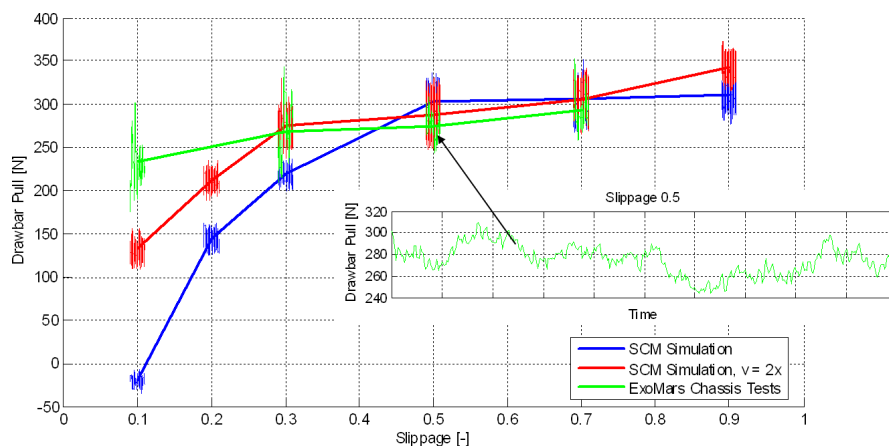


Fig. 16: Correlation of SCM simulations with ExoMars rover system level tests (drawbar pull)
Applied soil parameters: Mars soil simulant MSS-D [4]

6 Conclusion

In the paper a MBS-specific model for computing the contact forces between arbitrarily shaped contact objects and plastically deformable soil has been introduced. The kernel of the code is the discrete formulation of Bekker’s pressure-sinkage relationship and an algorithm for plastic soil deformation. After verification and validation (correlation) of the model two limiting factors in terms of simulation accuracy have been identified: 1) Discretization dependent errors and 2) errors caused by unknown contact velocity dependent soil parameters. The first problem can be solved choosing a high surface resolution of the contact partners at the cost of computation time. However, the second problem requires fundamental, experimental work like bevameter experiments with different penetration velocities in order to extract both, the required number of new velocity dependent parameters to be introduced and their soil specific values.

References

- [1] **M.G. Bekker**, *Introduction to Terrain-Vehicle Systems*, The University of Michigan Press, Ann Arbor, USA, 1969
- [2] **J.Y. Wong**, *Theory of Ground Vehicles*, Wiley, New York, 4th Edition, 2008
- [3] **W. Söhne**, *Agricultural Engineering and Terramechanics*, Journal of Terramechanics, Vol. 9, No. 4, 1969
- [4] **M. Scharringhausen**, *Martian, Terrestrial and Lunar Soil Parameters*, DLR, Internal Report, 2008
- [5] **S. Michaud, M. Höpflinger, T. Thuer, C. Lee, A. Krebs, B. Desmont, A. Gibbesch, L. Richter**, *Lessons Learned from ExoMars Locomotion System Test Campaign*, 10th Workshop on Advanced Space Technologies for Robotics and Automation, ESTEC, Noordwijk, The Netherlands, 2008
- [6] **Z. Janosi, B. Hanamoto**, *An Analysis of the Drawbar Pull vs Slip Relationship for Track Laying Vehicles*, Land Locomotion Laboratory, Report RR 47, 1961